Image Restoration Method for Deep-sea Tripod Observation Systems in the South China Sea

Huimin Lu[*], Yujie Li, Seiichi Serikawa
Dept. of Electronic and Electrical Engineering
Kyushu Institute of Technology
Fukuoka, Japan
[*]luhuimin@ieee.org

Jianru Li[**], Zhifei Liu
State Key Laboratory of Marine Geology
Tongji University
Shanghai, China
[**]lijianru@tongji.edu.cn

Xin Li[†]
State Key Laboratory of Ocean Engineering
Shanghai Jiaotong University
Shanghai, China
[†]lixin@sjtu.edu.cn

***Abstract*—The deep-sea tripod systems designed and built at the U.S. Geological Survey (USGS) Pacific Coastal and Marine Science Center (PCMSC) in Santa Cruz, California. They were recovered in late September 2014 after spending about half a year collecting data on the floor of the South China Sea. The Free-Ascending Tripod (FAT) was deployed at 2,100 meters water depth—roughly 10 times as deep as most tripods dedicated to measuring currents and sediment movement at the seafloor. Deployment at this unusual depth was made possible by the tripod's ability to rise by itself to the surface rather than being pulled up by a line. Instruments mounted on the tripod took bottom photographs and measured such variables as water temperature, current velocity, and suspended-sediment concentration. FAT is used to better understand how and where deep-seafloor sediment moves and accumulates. Besides of this, we also use them to study the deep-sea biology. The obtained the images from the camera, the biology animals are hardly to be distinguished. In this paper, we are concerned to use the image processing technology for recovering the deep-sea scene.**

Keywords*—*image restoration; deep-sea tripod; South China Sea; ocean observation

I. Introduction

Ocean observations [1] are being developed and deployed by scientists, researchers and institutions around the world oceans for monitoring the status of ocean. Some observatories are cabled, For example, the Ocean Networks Canada Observatory [2], contains VENUS and NEPTUNE Canada cabled networks. It enables real-time interactive experiments, for measuring ocean health, ecosystems, resources, natural hazards and marine conservation. Some observatories are moored or made up of surface buoys, such as NOAA Ocean Climate Observation System [3]. The observations near the equator are of particular important to climate. Besides of monitoring the air-water exchange of heat and water, the moored buoys provide platforms for instrumentation to measure the air-water exchange of carbon dioxide in the tropics. Some observatories are remote sensed, such as Japanese Ocean Flux Data Sets with Use of Remote Sensing Observation [4]. It is used for monitoring the changes of heat, water and momentum with atmosphere at ocean surface.

Interestingly, there are some excellent systems for ocean observing, such as Global Ocean Observing System proposed by Henry. Stommel WHOI [5]. More than 30 countries are joined in this program. However, until now this system also has some drawbacks. First, the system is not fully built-out because of funding issues. Second, most of subsystems are not at full operational capacity. Many of them are funded through research programs rather than operational. Third, deep ocean (under 2000 meters) is very under-sampled-issue of technology and cost.

In this paper, we firstly review the underwater imaging technologies. Then, analysis the feasibility of recent systems and propose some novel technologies for improving recent optical imaging systems.

II. Related work

Optical imaging sensors can be provided much information at high speed. They are commonly used in many terrestrial and air robotic application. However, because of the interaction between electromagnetic waves and water, optical imaging systems and vision systems need to be specifically designed to be able to use in underwater environment [6].

Underwater images have specific characteristics that should be consider during the gathering process and preprocessing process. Light attenuation, scattering, non-uniform lighting, shadows, color distortion, suspended particles or abundance of marine life on top or surrounding the target are frequently found in typical underwater scenes.

In this paper, we focus on a single image enhancement method. Single image enhancement is a challenging but ill-

978-0-933957-43-5 ©2015 MTS

posed problem. The obtained brightness of each pixel depends on the observed scene point radiance, scattering, attenuation, and ambient illumination. In reviewing recent studies, research related to underwater image enhancement can be classified into the following six main categories.

A. Polarization

Schechner et al. [7] restored images taken at significantly varied scene distances by using a polarization filter attached to a camera. A distance map of the scene was obtained by capturing two polarized images from different angles. Liang et al. [8] proposed a Stokes matrix-based four-angle rotation polarization filter to remove haze. However, these methods cannot attenuate the transmission of radiance through polarization filters or multiple exposures, especially for time variations that are adverse to visibility and illumination conditions.

B. Turbidity Medium

Narasimhan et al. [9] and Cozman et al. [10] analyzed a static scene by obtaining multiple images under different visibility conditions. Although they reported impressive results, a static camera and a significant change in media turbidity were required under constant illumination conditions.

C. Multi-lighting

Narasimham et al. [11] and Tsiotsios et al. [12] proposed the use of multiple lights to estimate the backscatter from a scene. Treibitz et al. [13] proposed fusing images obtained using two-directional illumination to create a single clearer image. However, it is difficult to recover the time variations adverse to visibility in the presence of floating turbidity sediments.

D. Scene Depth

Studies have calculated scene depth to solve the ambiguities in the visibility enhancement problem [14, 15]. These works made assumptions about the scene that necessitate either manual inputs or special structures. Generating these information is difficult in water.

E. HDR Fusion

Ancuti et al. [16] combined the Laplacian contrast, contrast, saliency, and exposure features of white-balanced and color-corrected images. They then utilized the exposure fusion algorithm to obtain the final result. However, several results were color shifted due to the exposure process; selecting the exposed images is difficult.

F. Prior Experience

Fattal et al. [17] estimated scene radiance and derived a transmission image using single-image statistics. He et al. [18] analyzed numerous natural sky images and determined that most color images contain a dark channel. On the basis of this finding, they proposed a dark channel prior dehazing algorithm. The subsequent image enhancement resulted in regional contrast stretching that could cause halos or aliasing. Moreover, the dark channel assumption is based on natural outdoor image statics that might not hold in arbitrary underwater scenes.

III. Image Restoration System

In this project, we built the image restoration system by four parts. That is, image descattering, illumination correction, color correction, and super resolution. We will discuss each subsystem in details as following.

A. Image Descattering

Atmospheric light and artificial light traveling through water are sources of illumination for underwater environment. Let us suppose that the energy attenuation model can be formulated as follows [19]:

$$E_\lambda^W(x) = E_\lambda^A(x) \cdot Nrer(\lambda)^{D(x)} + E_\lambda^I(x) \cdot Nrer(\lambda)^{T(x)}, \quad \lambda \in \{r,g,b\}, \tag{1}$$

where $E_\lambda^W(x)$ is the amount of illumination at point x, $E_\lambda^A(x)$ is the amount of illumination of atmospheric light at point x, $E_\lambda^I(x)$ is the illumination of artificial light at point x, and *Nrer* is the normalized residual energy ratio [20]. In general underwater environment, *Nrer* has the following values:

$$N_{rer}(\lambda) = \begin{cases} 0.8 \sim 0.85 & if\ \lambda = 650 \sim 750\mu m(red) \\ 0.93 \sim 0.97 & if\ \lambda = 490 \sim 550\mu m(green) \\ 0.95 \sim 0.99 & if\ \lambda = 400 \sim 490\mu m(blue) \end{cases}. \tag{2}$$

At point x, the artificial light is reflected at a distance $T(x)$ to the camera. $D(x)$ is the depth from water surface to scene. Color distortion and scattering occurs in this process. Supposing that the absorption and scattering rate is $\rho_\lambda(x)$, the illumination of ambient light $E_\lambda^\omega(x)$ is

$$E_\lambda^\omega(x) = \left(E_\lambda^A(x) \cdot Nrer(\lambda)^{D(x)} + E_\lambda^I(x) \cdot Nrer(\lambda)^{T(x)}\right) \cdot \rho_\lambda(x), \quad \lambda \in \{r,g,b\}. \tag{3}$$

As the modified dehazing model, the scene image $I_\lambda(x)$ formed at the camera can be formulated as follows:

$$I_\lambda(x) = \left[\left(E_\lambda^A(x) \cdot Nrer(\lambda)^{D(x)} + E_\lambda^I(x) \cdot Nrer(\lambda)^{T(x)}\right) \cdot \rho_\lambda(x)\right] \cdot t_\lambda(x) + (1 - t_\lambda(x)) \cdot B_\lambda, \ \lambda \in \{r,g,b\}, \tag{4}$$

where the homogenous background B_λ represents the part of the light reflected by the object, The residual energy ratio $t_\lambda(x)$ can be represented in terms of the energy of a light beam of wavelength λ before and after it propagates through transmission $T(x)$ within the water, it is represented by $E_\lambda^{residual}(x)$ and $E_\lambda^{initial}(x)$, respectively, as follows:

$$t_\lambda(x) = \frac{E_\lambda^{residual}(x)}{E_\lambda^{initial}(x)} = 10^{-\beta(\lambda) T(x)} = Nrer(\lambda)^{T(x)}, \tag{5}$$

where the normalized residual energy ratio $N_{rer}(\lambda)$ corresponds to the ratio of residual energy to initial energy for every unit of distance propagated, and $\beta(\lambda)$ is the extinction coefficient of the medium.

Consequently, substituting Eq. (5) in Eq. (4), we obtain:

$$I_\lambda(x)=\left[\begin{pmatrix} E_\lambda^A(x)\cdot Nrer(\lambda)^{D(x)}+ \\ E_\lambda^I(x)\cdot Nrer(\lambda)^{T(x)} \end{pmatrix}\cdot\rho_\lambda(x)\right]\cdot Nrer(\lambda)^{T(x)} \\ +\left(1-Nrer(\lambda)^{T(x)}\right)\cdot B_\lambda,\ \lambda\in\{r,g,b\}. \tag{6}$$

The above equation contains the light scattered and the wavelength attenuation. Once water surface-scene depth $D(x)$ and transmission $T(x)$ are known, a clean image can be recovered. Figure. 1 shows a schematic of the proposed model. In order to improve image quality, we consider the processing flowchart shown in Fig.1.

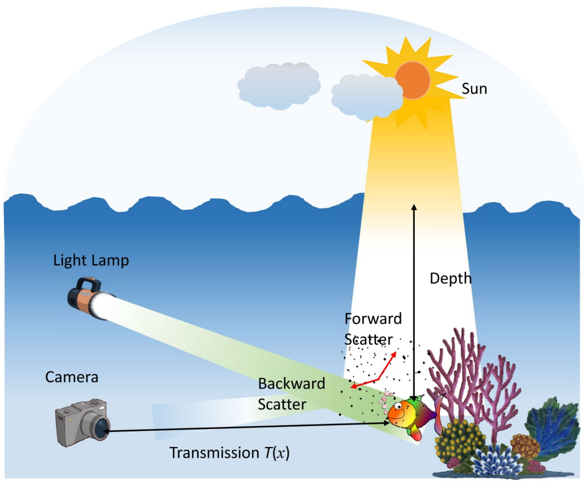

Fig. 1. Schematic of the underwater imaging model.

As indicated in Eq. (6), we suppose the non-scatter image $J_\lambda(x)$ reflected from point x is

$$J_\lambda(x)=\left(E_\lambda^A(x)\cdot Nrer(\lambda)^{D(x)}+E_\lambda^I(x)\cdot Nrer(\lambda)^{T(x)}\right)\cdot\rho_\lambda(x), \\ \lambda\in\{r,g,b\}. \tag{7}$$

We define the underwater dark channel $J_{dark}(x)$ for the underwater non-scatter image $J_\lambda(x)$ as

$$J_{dark}(x)=\min_\lambda \min_{y\in\Omega(x)} J_\lambda(y),\ \lambda\in\{r,b\}. \tag{8}$$

If point x is at a part of the foreground object, the value of the minimum dual channel is very small [34]. Applying the min operation to a local patch $\Omega(x)$ on the scattered image $I_\lambda(x)$, we have

$$\min_{y\in\Omega(x)}\left(I_\lambda(y)\right)=\min_{y\in\Omega(x)}\begin{Bmatrix} J_\lambda(y)\cdot Nrer(\lambda)^{T(y)}+ \\ \left(1-Nrer(\lambda)^{T(y)}\right)\cdot B_\lambda \end{Bmatrix}, \\ \lambda\in\{r,b\}. \tag{9}$$

Because B_λ is the homogeneous background light and the residual energy ratio $Nrer(\lambda)^{T(y)}$ on the small local patch $\Omega(x)$ surrounding point x is essentially a constant $Nrer(\lambda)^{T(x)}$, the min operation on the second term on the right-hand side of Eq. (9) can be removed to obtain

$$\min_{y\in\Omega(x)}\left(I_\lambda(y)\right)=\min_{y\in\Omega(x)} J_\lambda(y)\cdot Nrer(\lambda)^{T(x)}+ \\ \left(1-Nrer(\lambda)^{T(x)}\right)\cdot B_\lambda,\ \lambda\in\{r,b\}. \tag{10}$$

We rearrange the above equation and perform on more min operation among all channels as follows:

$$\min_\lambda\left\{\frac{\min_{y\in\Omega(x)}\left(I_\lambda(y)\right)}{B_\lambda}\right\}= \\ \min_\lambda\left\{\frac{\min_{y\in\Omega(x)}J_\lambda(y)}{B_\lambda}\cdot Nrer(\lambda)^{T(x)}\right\}+ \\ \min_\lambda\left(1-Nrer(\lambda)^{T(x)}\right),\ \lambda\in\{r,b\}. \tag{11}$$

The first term on the right-hand side of Eq. (11) is a dark channels equal to 0. Consequently, the estimated transmission is as following.

$$\max_\lambda\left(Nrer(\lambda)^{T(x)}\right)=1-\min_\lambda\left\{\frac{\min_{y\in\Omega(x)}\left(I_\lambda(y)\right)}{B_\lambda}\right\},\lambda\in\{r,b\}. \tag{12}$$

Finally, the transmission $T(x)$ can be represented as following.

$$T(x)=\ln\left(1-\min_\lambda\left\{\frac{\min_{y\in\Omega(x)}\left(I_\lambda(y)\right)}{B_\lambda}\right\}\right)/\ln\max\{Nrer(\lambda)\},\lambda\in\{r,b\}. \tag{13}$$

After obtained the transmission, we can recover the real scene by descattering model [20].

B. Illuminaction Correction

In the underwater environment, we must use artificial light for imaging. However, it will cause the vignetting effect. In [21], K. Sooknanan et al. proposed a multi-frame vignetting correction model for removing the vignetting phenomenon which involves estimating the light source footprint on the seafloor. This artificial light correction can well done, however, it cost large time for computing. So, in this paper, we intend to introduce a signal frame-based vignette removal method. Given the fact that we are interested in the overall effect of light attenuation through the system and not all of the image formation details, we have derived an effective degradation model, $Z(r,\theta)$ as follows,

$$Z(r,\theta)=O(r,\theta)V(r) \tag{14}$$

where Z is the image with vignetting, O is the vignetting-free image, and V is the vignetting function. Our goal is to find the optimal vignetting function V that minimizes asymmetry of the radial gradient distribution. By taking the log of Eq.(14), we get

$$\ln(Z(r,\theta)=\ln O(r,\theta)+\ln V(r) \tag{15}$$

Let $\mathbf{Z}$=ln$Z$, $\mathbf{O}$=ln$O$, and $\mathbf{V}$=ln$V$. We denote the radial gradients of $\mathbf{Z}$, $\mathbf{O}$, and $\mathbf{V}$ for each pixel (r, θ) by $R_r^{\mathbf{Z}}(r,\theta)$, $R_r^{\mathbf{O}}(r,\theta)$, $R_r^{\mathbf{V}}(r,\theta)$. Then,

$$\mathrm{R}_r^{\mathbf{Z}}(r,\theta) = \mathrm{R}_r^{\mathbf{O}}(r,\theta) + \mathrm{R}_r^{\mathbf{V}}(r,\theta) \quad (16)$$

Given an image **Z** with vignetting, we find a maximum a posterior (MAP) solution to **V**. Taking Bayes rule, we get,

$$\mathbf{V} = \arg\max_{\mathbf{V}} P(\mathbf{V} \mid \mathbf{Z}) \sim \arg\max_{\mathbf{V}} P(\mathbf{Z} \mid \mathbf{V}) P(\mathbf{V}) \quad (17)$$

Considering the vignetting function at discrete, evenly sampled radii: ($\mathbf{V}(r_t)$, $r_t \in S_r$), where $S_r = \{ r_0, r_1, \ldots, r_{n-1} \}$. Each pixel ($r$, θ) is associated with the sector in it resides, and sector width is δr. The vignetting function is in general smooth, therefore, we obtain,

$$P(\mathbf{V}) = e^{-\lambda_s \sum_{r_t \in S_r} \mathbf{V}''(r_t)^2} \quad (18)$$

where λ_s is chosen to compensate for the noise level in the image, and $\mathbf{V}''(r_t)$ is approximated as

$$\mathbf{V}''(r_t) = \frac{\mathbf{V}(r_{t-1}) - 2\mathbf{V}(r_t) + \mathbf{V}(r_{t+1})}{(\delta r)^2} \quad (19)$$

Using the sparsity prior method on the vignetting-free image **O**,

$$P(\mathrm{Z} \mid \mathrm{V}) = P(R_r^{\mathrm{O}}) = e^{-|R_r^{\mathrm{O}}|^{\alpha}}, \ \alpha<1 \quad (20)$$

Substituting Eq.(16) and Eq.(20), we have

$$P(\mathbf{Z} \mid \mathbf{V}) = e^{-\sum_{(r,\theta)} |\mathrm{R}_r^{\mathbf{Z}}(r,\theta) - \mathrm{R}_r^{\mathrm{V}}(r)|^{\alpha}} \quad (21)$$

The overall energy function $P(\mathbf{Z}|\mathbf{V})P(\mathbf{V})$ can be written as

$$E = \sum_{(r,\theta)} |\mathrm{R}_r^{\mathbf{Z}}(r,\theta) - \mathrm{R}_r^{\mathrm{V}}(r)|^{\alpha} + \lambda_s \sum_{r_t \in S_r} \mathbf{V}''(r_t)^2 \quad (22)$$

Through minimize E, we can estimate the $\mathbf{V}(r_t)$. Then, we use the IRLS technique for estimating the vignetting function.

C. Color Correction

We take the chromatic transfer function [22] τ for weighting the light from the surface to a given depth of objects as

$$\tau_{\lambda} = \frac{E_{\lambda}^{surface}}{E_{\lambda}^{object}} \quad (23)$$

where the transfer function τ at wavelength λ is derived from the irradiance of the surface $E_{\lambda}^{surface}$ by the irradiance of the object E_{λ}^{object}. According to the spectral response of RGB camera, we convert the transfer function to RGB domain:

$$\tau_{RGB} = \sum^{k} \tau_{\lambda} \cdot C_b(\lambda) \quad (24)$$

where the weighted RGB transfer function is τ_{RGB}, $C_b(\lambda)$ is the underwater spectral characteristic function of colour band b, $b \in \{r,g,b\}$. k is the number of discrete bands of the camera spectral characteristic function.

Finally, the corrected image is gathered from the weighted RGB transfer function by

$$J_{\lambda}(x) = \hat{J}_{\lambda}(x) \cdot \tau_{RGB} \quad (25)$$

where $J_{\lambda}(x)$ and $\hat{J}_{\lambda}(x)$ are respectively the color corrected and uncorrected images.

D. Super-resolution

For underwater imaging, scatter and noise corruption is a ubiquitous phenomenon that affects image processing tasks. The conventional approaches [23] were previously exploited for noise-cleaning using 'Non-Local Means' [24] or BM3D [25], as well as a regularization prior for inverse problems [26]. A related SR approach was proposed by [27] for obtaining higher-resolution video frames, by applying the SR constraints to similar patches. However, during Singh et al.'s work [28], although both denoising and SR use patch similarity based priors, they are used towards different objectives. The denoising operation is to smooth a large number of similar patches so as to remove noise in the patch. The goal of SR is to seek more similar patches at different scales to enhance the textural content of each patch. So, they overcome the signal loss caused by denoising by simultaneous SR and denoising method [29].

IV. EXPERIMENTS AND DISCUSSIONS

Ten underwater images were selected, including five images from the project "South China Sea Deep" and five images from our water tank experiments. The water tank contains 180 L water (90 cm × 45 cm × 45 cm). Both the underwater lights (INON LEs) and the underwater camera (OLYMPUS μTough TG2) were placed in the water [30]. The objects were placed 30 cm deep. The distance between the objects and the camera was approximately 60 cm. We executed the proposed algorithm on the selected images. The performance of the proposed algorithm is evaluated both analytically and experimentally by using ground truths. We also compare the proposed method with other currently proposed state-of-the-art methods. The results demonstrate that the proposed method shows superior scatter removal and color correction capabilities.

A. Water Tank Simulation

At the first evaluation, we made a linear scale of five turbidity steps ranging from clean to heavily scattered by adding deep sea soil to the seawater (from 0.6 to 100 mg/L). Fig.2 shows the results.

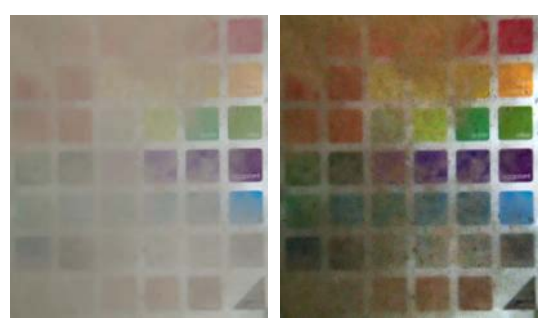

(a) (b)

(c)

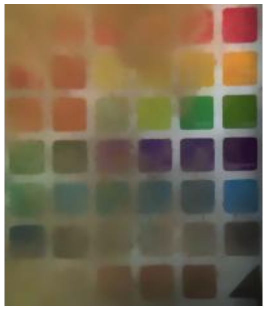

(d)

(e)

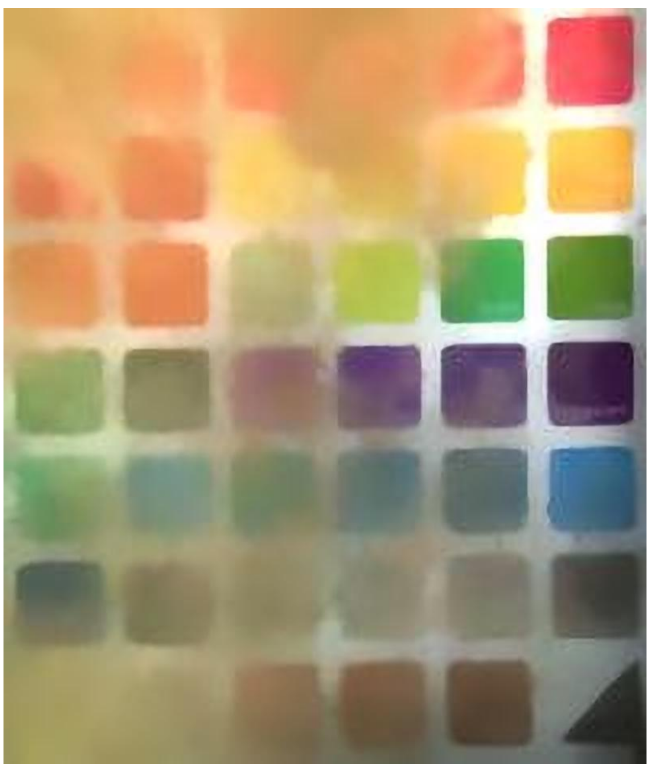

(f)

Fig. 2. Results of water tank experiment. (a) Input image. (b) Descattered result. (c) Illumination corrected result. (d) Denoised result. (e) Color corrected result. (f) Super-resolved result (4×).

B. Real-world Experiment

We also test the proposed method with the images of real-world, deep-sea observation systems. The image used was captured by the Free-Ascending Tripod (FAT), which was built at the U.S. Geological Survey (USGS) Pacific Coastal and Marine Science Center (PCMSC) in Santa Cruz, California and is used to monitor in-situ sediment movement. FAT was recovered in late September 2014 after spending about half a year collecting data on the floor of the northeastern South China Sea (SCS). Fig. 3 shows the result of each step.

(a)

(b)

(c)

(d)

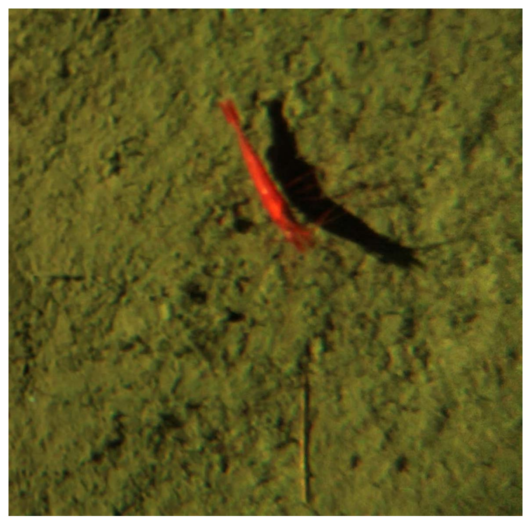

(e)

Fig. 3. Results of deep-sea image processing. (a) Captured image. (b) Illumination corrected result. (c) Denoised result. (d) Color corrected result. (e) Super-resolved result (4×).

V. CONCLUSION

In this paper, we built an image restoration system for in-suit deep sea observing in the South China Sea. The proposed scheme can improve the quality of deep-sea images well. It can remove the unwanted particles, can correct the non-uniform illumination as well as recover the real scene color, and super resolving the images. Water tank experiments and sea water experiments demonstrate that the proposed system performs better. The proposed methods are suitable for ocean observing.

. In future work, we need to design novel algorithms for large particles scatter removal.

ACKNOWLEDGMENT

This work was supported by Grant in Aid for Foreigner Research Fellows of Japan Society for the Promotion of Science (No.15F15077), Open Fund of the Key Laboratory of Marine Geology and Environment in Chinese Academy of Sciences (No.MGE2015KG02), Open Research Fund of State Key Laboratory of Marine Geology in Tongji University (MGK1407), and Open Research Fund of State Key Laboratory of Ocean Engineering in Shanghai Jiaotong University (OEK1315).

REFERENCES

[1] Ocean Observations, http://en.wikipedia.org/wiki/ocean_observations

[2] Ocean Networks Canada, http://www.oceannetworks.ca/

[3] NOAA Ocean Climate Observation Program, http://www.oco.noaa.gov/

[4] Japanese Ocean Flux Data Sets with Use of Remote Sensing Observation, http://dtsv.scc.u-tokai.ac.jp/j-ofuro/

[5] Woods Hole Oceanographic Institution, http://www.whoi.edu/

[6] H. Lu, Y. Li, L. Zhang, S. Serikawa, “Contrast enhancement for images enhancement in turbid water,” Journal of Optical Society of America A, vol.32, no.5, pp.886-893, 2015.

[7] Y. Schechner, and N. Karpel, “Recovery of underwater visibility and structure by polarization analysis,” IEEE Journal of Oceanic Engineering, vol.30, no.3, pp. 570–587, 2005.

[8] J. Liang, L. Ren, H. Ju, E. Qu, and Y. Wang, “Visibility enhancement of haze images based on a universal polarimetric imaging method,” Journal of Applied Physics, vol.116, no.17, pp. 1731071-1731077, 2014.

[9] S. Narasimhan and S. Nayar, “Contrast restoration of weather degraded images,” IEEE Transactions on Pattern Analysis and Machine Intelligence, vol.25, no.6, pp.713–724, 2003.

[10] F. Cozman and E. Krotkov, “Depth from scattering,” in Proceedings of IEEE Conference on Computer Vision and Pattern Recognition, pp. 801–806, 1997.

[11]

[12] C. Tsiotsios, M. Angelopoulou, T. Kim, and A. Davison, “Backscatter compensated photometric stereo with 3 sources,” in Proceedings of IEEE Conference on Computer Vision and Pattern Recognition, pp. 4321–4328, 2014.

[13] T. Treibitz and Y. Schechner, “Turbid scene enhancement using multi-directional illumination fusion,” IEEE Transactions on Image Processing, vol.21, no.11, pp.4662–4667, 2012.

[14] N. Hautiere, J.P. Tarel, and D. Aubert, “Towards fog-free in-vehicle vision systems through contrast restoration,” in Proceedings of IEEE Conference on Computer Vision and Pattern Recognition, pp. 1–8, 2008.

[15] J. Kopf, B. Neubert, B. Chen, M. Cohen, D. Cohen-Or, O. Deussen, M. Uyttendaele, and D. Lischinski, “Deep photo: Model-based photograph enhancement and viewing,” ACM Transaction on Graphics, vol.27, no.5, pp.116:1–116:10, 2008.

[16] C. Ancuti, C. O. Ancuti, T. Haber, and P. Bekaert, “Enhancing underwater images and videos by fusion,” in Proceedings of IEEE Conference on Computer Vision and Pattern Recognition, pp. 81–88, 2012.

[17] R. Fattal. “Single image dehazing,” ACM Transaction on Graphics, vol.27, no.3, pp. 1–8, 2008.

[18] K. He, J. Sun, and X. Tang, “Single image haze removal using dark channel prior,” IEEE Transactions on Pattern Analysis and Machine Intelligence, vol.33, no.12, pp. 2341–2353, 2011.

[19] H. Lu, Y. Li, and S. Serikawa, “Underwater image enhancement using guided trigonometric bilateral filter and fast automation color correction,” in Proceedings of IEEE International Conference on Image Processing, pp. 3412–3416, 2013.

[20] S. Grabtchak, T. J. Palmer, I. A. Vitkin, and W. M. Whelan, “Radiance detection of non-scattering inclusions in turbid media,” Biomedical Optics Express, vol.3, no.11, pp. 3001–3011, 2012.

[21] K. Sooknanan, A. Kokaram, D. Corrigan, “Improving underwater visibility using vignetting correction,” in Proceedings of SPIE, pp.83050M-1-8, 2012.

[22] D.L. Bongiorno, M. Bryson, D.G. Dansereau, S.B. Williams, “Spectral characterization of COTS RGB cameras using a linear variable edge filter,” in Proceedings of SPIE-IS&T, vol.86600N, pp.1-8, 2013..

[23] D. Glasner, S. Bagon, and M. Irani, “Super-resolution from a single image,” in Proceedings of IEEE International Conference on Computer Vision, pp.349-356, 2009.

[24] A. Buades, B. Coll, and J.M. Morel, “A non-local algorithm for image denoising,” in Proceedings of IEEE Conferernce on Computer Vision and Pattern Recognition, pp.60-65, 2005.

[25] K. Dabov, A. Foi, V. Katkovnik, and K. Egiazarian, “Image denoising by sparse 3d transform domain collaborative filtering,” IEEE Transactions on Image Processing, vol.16, no.8, pp.2080-2095, 2007.

[26] G. Peyre, S. Bougleux, and L.D. Cohen, “Non-local regularization of inverse problems,” in Proceedings of Europen Conferernce on Computer Vision, pp.57-68, 2008.

[27] M. Potter, M. Elad, H. Takeda, and P. Milanfar, “Generalizing the nonlocal-means to super-resolution reconstruction,” IEEE Transactions on Image Processing, vol.18, no.1, pp.36-51, 2008.

[28] A. Singh, F. Porkili, and N. Ahuja, “Super-resolving noisy images,” in Proceedings of IEEE Conferernce on Computer Vision and Pattern Recognition, pp.2846-2853, 2014.

[29] J.B. Huang, A. Singh, and N. Ahuja, “Single image super-resolution using transformed self-exemplars,” in Proceedings of IEEE Conference on Computer Vision and Pattern Recognition, pp.1-10, 2015.

[30] S. Serikawa, H. Lu, “Underwater image dehazing using joint trilateral filter,” Computers and Electrical Engineering, vol.40, no.1, pp.41-50, 2014.